

InGaN/GaN multiple-quantum-well light-emitting diodes with a grading InN composition suppressing the Auger recombination

Zi-Hui Zhang, Wei Liu, Zhengang Ju, Swee Tiam Tan, Yun Ji, Zabu Kyaw, Xueliang Zhang, Liancheng Wang, Xiao Wei Sun, and Hilmi Volkan Demir

Citation: *Applied Physics Letters* **105**, 033506 (2014); doi: 10.1063/1.4891334

View online: <http://dx.doi.org/10.1063/1.4891334>

View Table of Contents: <http://scitation.aip.org/content/aip/journal/apl/105/3?ver=pdfcov>

Published by the AIP Publishing

Articles you may be interested in

On the uncertainty of the Auger recombination coefficient extracted from InGaN/GaN light-emitting diode efficiency droop measurements

Appl. Phys. Lett. **106**, 101101 (2015); 10.1063/1.4914833

High efficiency InGaN/GaN light emitting diodes with asymmetric triangular multiple quantum wells

Appl. Phys. Lett. **104**, 091111 (2014); 10.1063/1.4867023

Effect of V-defects on the performance deterioration of InGaN/GaN multiple-quantum-well light-emitting diodes with varying barrier layer thickness

J. Appl. Phys. **114**, 143706 (2013); 10.1063/1.4824801

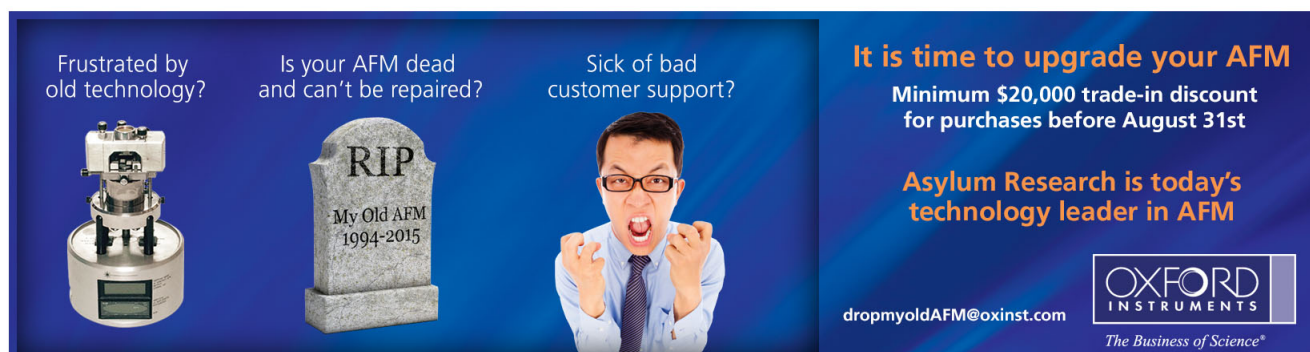
Modulation bandwidth studies of recombination processes in blue and green InGaN quantum well micro-light-emitting diodes

Appl. Phys. Lett. **102**, 091103 (2013); 10.1063/1.4794078


Direct measurement of auger recombination in In 0.1 Ga 0.9 N / GaN quantum wells and its impact on the efficiency of In 0.1 Ga 0.9 N / GaN multiple quantum well light emitting diodes

Appl. Phys. Lett. **95**, 201108 (2009); 10.1063/1.3266520


Frustrated by old technology?



Is your AFM dead and can't be repaired?



Sick of bad customer support?



It is time to upgrade your AFM

Minimum \$20,000 trade-in discount for purchases before August 31st

Asylum Research is today's technology leader in AFM

dropmyoldAFM@oxinst.com



The Business of Science®

InGaN/GaN multiple-quantum-well light-emitting diodes with a grading InN composition suppressing the Auger recombination

Zi-Hui Zhang,^{1,a)} Wei Liu,^{1,a)} Zhengang Ju,¹ Swee Tiam Tan,¹ Yun Ji,¹ Zabu Kyaw,¹ Xueliang Zhang,¹ Liancheng Wang,¹ Xiao Wei Sun,^{1,b)} and Hilmi Volkan Demir^{1,2,b)}

¹LUMINOUS! Centre of Excellence for Semiconductor Lighting and Displays, School of Electrical and Electronic Engineering, School of Physical and Mathematical Sciences, Nanyang Technological University, 50 Nanyang Avenue, Singapore 639798

²Department of Electrical and Electronics, Department of Physics, and UNAM-Institute of Material Science and Nanotechnology, Bilkent University, TR-06800 Ankara, Turkey

(Received 3 May 2014; accepted 14 July 2014; published online 23 July 2014)

In conventional InGaN/GaN light-emitting diodes (LEDs), thin InGaN quantum wells are usually adopted to mitigate the quantum confined Stark effect (QCSE), caused due to strong polarization induced electric field, through spatially confining electrons and holes in small recombination volumes. However, this inevitably increases the carrier density in quantum wells, which in turn aggravates the Auger recombination, since the Auger recombination scales with the third power of the carrier density. As a result, the efficiency droop of the Auger recombination severely limits the LED performance. Here, we proposed and showed wide InGaN quantum wells with the InN composition linearly grading along the growth orientation in LED structures suppressing the Auger recombination and the QCSE simultaneously. Theoretically, the physical mechanisms behind the Auger recombination suppression are also revealed. The proposed LED structure has experimentally demonstrated significant improvement in optical output power and efficiency droop, proving to be an effective solution to this important problem of Auger recombination. © 2014 AIP Publishing LLC.

[<http://dx.doi.org/10.1063/1.4891334>]

Both electrically and optically, InGaN/GaN light-emitting diodes (LEDs) have promised higher efficiency and reliability as the blue light sources for white light generation. Hence, they are regarded as excellent candidates for artificial lighting to replace the incumbent conventional fluorescent and incandescent lighting sources. For that a significant progress has been made for InGaN/GaN LEDs in the past several decades.¹ However, the LED efficiency has been so far still limited and especially high levels of efficiency droop have commonly been observed at high current density, caused by several factors including electron overflow,^{2,3} Shockley-Read-Hall (SRH) recombination,^{4,5} and Auger recombination.⁶ Among them, the Auger recombination is more severe under a high injection current level, since the Auger recombination scales with the third power of the carrier density ($\sim n^3$ with n denoted as the density of the captured carriers in quantum wells). Therefore, it is very important to suppress the Auger recombination to improve the LED performance. To address the Auger-related issues and enhance the LED performance, one can consider increasing the quantum well thickness and homogenizing the carrier distribution within the quantum wells to reduce the carrier density. Nevertheless, InGaN/GaN LEDs grown along the [0001] orientation suffer from the strong polarization induced electric field in the quantum wells.⁷ Consequently, a tilted energy band alignment is produced, which in turn causes electron and hole separation and carrier accumulation at the opposite interfaces of the polarization mismatched

quantum well and quantum barrier heterojunction. A more homogeneous carrier distribution can be realized by the LED structures based on nonpolar and semipolar growth planes.^{8,9} Moreover, even in the case of the [0001] orientation, the polarization matched condition can be realized by embedding InGaN quantum wells between the properly alloyed quaternary AlGaInN quantum barriers.¹⁰ However, the cost of the nonpolar/semipolar substrates and the limited freedom of epitaxial growth for the quaternary AlGaInN compounds hinder the wide adoption of these solutions. On the other hand, due to the mobility and doping asymmetry for electrons and holes, the electron density is normally higher than the hole density in the quantum wells, and hence the Auger recombination can be effectively reduced if the electrons are evenly distributed in the quantum wells under high current injection level.

In this work, we proposed and demonstrated a LED architecture grown along the [0001] orientation with wide quantum well thickness of grading InN composition in the InGaN/GaN quantum wells. We achieved an enhanced level of optical power and a reduced efficiency droop both in numerical simulations and experimental measurements, which is well attributed to the Auger recombination rate suppression by the proposed structure. The computations show a more flattened conduction band and a more even electron distribution profile in the quantum wells for the proposed LED. The Auger recombination is found to be less supported in the proposed LED structure according to our calculations.

The LEDs (samples A and B) with the aforementioned quantum well configurations have been grown by a metal-organic chemical vapor deposition (MOCVD) system. The growth for both the samples was initiated from the c-plane

^{a)}Z.-H. Zhang and W. Liu contributed equally to this work.

^{b)}Electronic addresses: EXWSUN@ntu.edu.sg and VOLKAN@stanfordalumni.org

sapphire substrates. A 30 nm thick GaN nucleation layer was first deposited and then a 4 μm thick unintentionally doped GaN (u-GaN) layer was grown as the template. This was followed by a 2 μm n-type GaN layer, which was doped by Si dopants of $5 \times 10^{18} \text{ cm}^{-3}$. The two grown epi-samples differ only in their multiple quantum wells (MQWs). Sample A employed three periods of $\text{In}_{0.15}\text{Ga}_{0.85}\text{N}/\text{GaN}$ MQWs of which the quantum well and quantum barrier thickness was fixed at 3 nm and 12 nm, respectively. Sample B also employed three periods of InGaN/GaN MQWs, but the quantum well thickness was increased to 5 nm and the InN composition was linearly decreased from 0.15 to 0.08 within the 5 nm quantum well range. The quantum barrier thickness was kept as 12 nm. Note that the average InN composition of the quantum well of sample B was set to 0.115 in order to keep the same 450 nm peak emission wavelength (W_p) as that of sample A. The schematic energy band diagrams of the quantum well for samples A and B have been illustrated in Figs. 1(a) and 1(b), respectively. Subsequently, a 25 nm p-type $\text{Al}_{0.20}\text{Ga}_{0.80}\text{N}$ electron blocking layer and a 0.2 μm thick p-type GaN layer were grown for both the samples. The effective hole concentration was estimated to be $3 \times 10^{17} \text{ cm}^{-3}$. Finally, a heavily doped p^+ -GaN layer of 10 nm was finally grown serving as the ohmic contact layer.

For optical output power characterization of samples A and B, an integrating sphere attached to an Ocean Optics spectrometer (QE65000) was used to collect the electroluminescence (EL). The indium metal contacts with a diameter of 1.0 mm were made on the LED wafers. Also, the numerical simulations were conducted to study the electron density profile, the energy bands, and the carrier recombination. The software package used in this work is the commercial APSYS simulator.¹¹ The SRH recombination coefficient, the

energy band offset, and the other simulation parameters for nitrogen-containing compounds can be found in our previously published works.^{7,11–15} Meanwhile, according to Figs. 1(a) and 1(b), we also considered the polarization induced charges, and the charge density is calculated according to the models developed by Fiorentini *et al.*¹⁶ Specifically, a bulk charge density of $+5.15 \times 10^{24} \text{ m}^{-3}$ was assumed in the $\text{In}_{0.15} \rightarrow 0.08\text{Ga}_{0.85} \rightarrow 0.92\text{N}/\text{GaN}$ MQWs for sample B¹⁷ while the polarization induced interface charge density for $\text{In}_{0.15}\text{Ga}_{0.85}\text{N}/\text{GaN}$ and $\text{In}_{0.08}\text{Ga}_{0.92}\text{N}/\text{GaN}$ heterojunctions was set to 0.54×10^{17} and $0.30 \times 10^{17} \text{ m}^{-2}$, respectively, for both samples A and B. The screening effect to the polarization induced electric field in the quantum well by the free carriers has also been taken into account during the computations. The Auger recombination coefficients were taken from the recently published work by Kioupakis *et al.*⁶ Note that we did not consider the impact of the polarization effect on the SRH and Auger recombination coefficients,¹⁸ since it has only minor effect on the simulation results.

Figs. 2(a)–2(d) show the optical output power and the external quantum efficiency (EQE) for samples A and B both from the computations and the experiments. It can be seen that both the optical output power and the EQE are improved for sample B compared to sample A and a good agreement between the numerical and experimental results are observed. Specifically, according to Fig. 2(c) the experimentally measured optical output power for sample B at 150 A/cm^2 is increased by 29.39% when compared to that for sample A. In addition, sample B has demonstrated a reduced efficiency droop both in the computation and the experiment according to Figs. 2(b) and 2(d). The numerically calculated efficiency droop for samples A and B in Fig. 2(b) is 40.73% and 35.52% at 150 A/cm^2 , respectively; while the experimentally measured droop for samples A and B in Fig. 2(d) is 39.23% and 31.83% at 150 A/cm^2 , respectively. In addition, the values of the full width at half maximum (FWHM) in terms of the current density for the EL spectra are also shown as an inset in Fig. 2(d). The FWHM for sample B is slightly larger than that for sample A. However, such a small variation in the FWHM values between the two samples will not cancel the advantage of the proposed quantum well structure in improving the LED performance. Hence, the reduced efficiency droop for sample B is attributed to the suppressed Auger recombination rates within the proposed quantum wells, and the details are to be discussed subsequently. Note that the slight discrepancy between the computed and measured results is likely due to the uncertainty and discrepancy for the relationship between the simulation parameters and temperature/carrier density for III-nitride materials.¹⁹

The computed energy band diagrams for samples A and B at 140 A/cm^2 are demonstrated in Figs. 3(a) and 3(b), respectively. Fig. 3(a) clearly shows that the conduction band of each quantum well has been significantly tilted and the electrons are strongly accumulated locally at the interface of the quantum well and the quantum barrier, which adversely promotes the Auger recombination rates within the quantum wells. However, the conduction band of the quantum wells is more flattened in sample B, as a result of the InN composition linearly decreased from 0.15 to 0.08 in

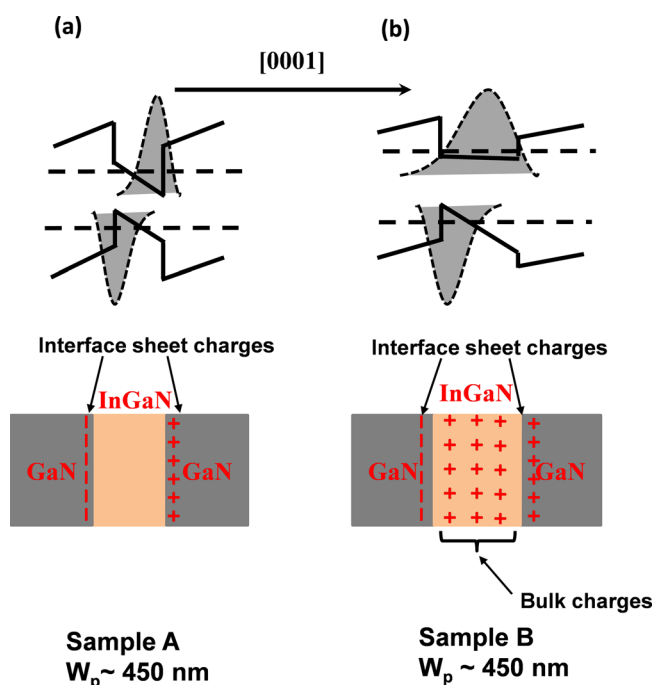


FIG. 1. Schematic energy diagrams for the quantum well region of (a) the conventional LED sample A and (b) the proposed LED sample B with wide quantum well and InN composition linearly decreasing along the [0001] growth orientation.

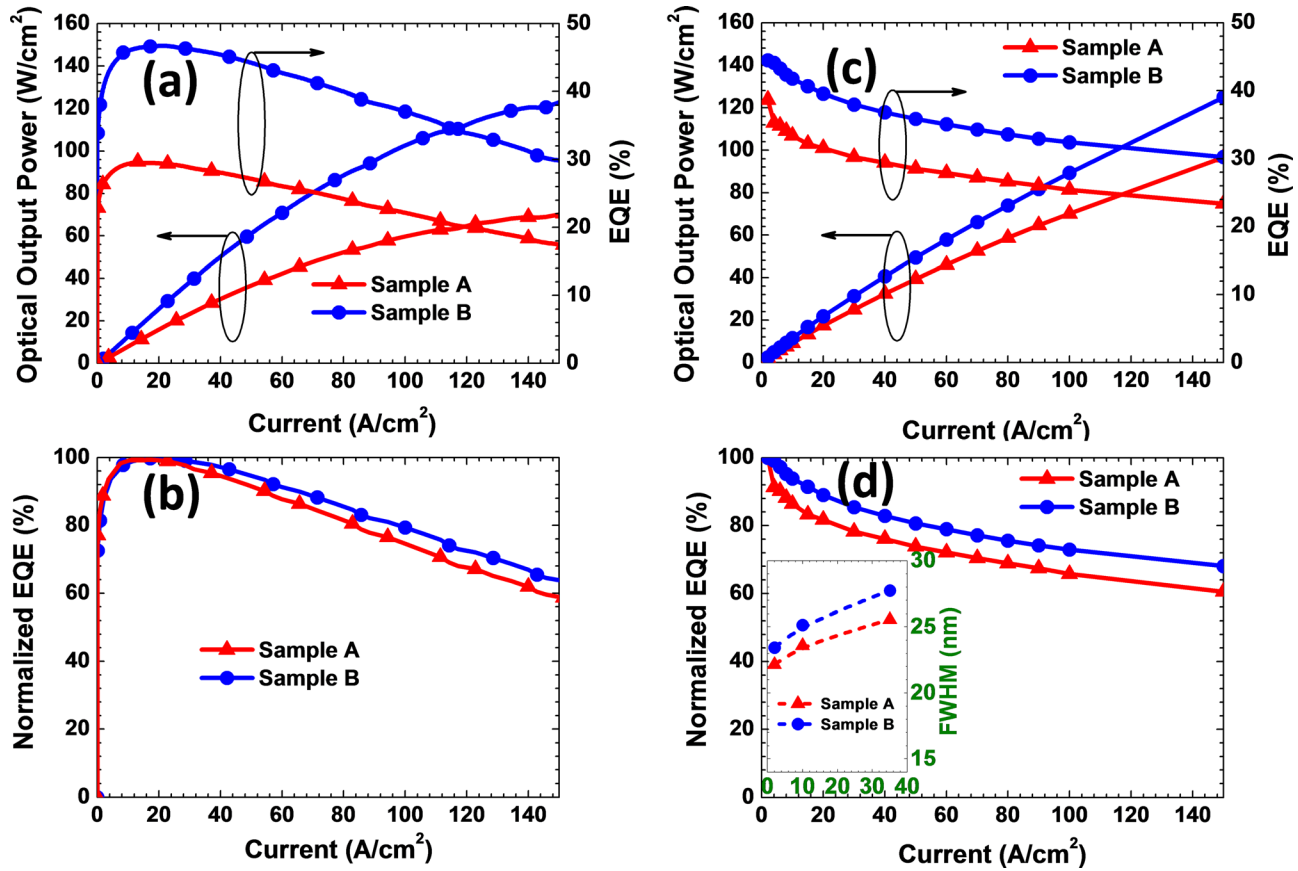


FIG. 2. (a) Numerically computed optical output power and EQE, (b) calculated normalized EQE, (c) experimentally measured optical output power and EQE, and (d) measured normalized EQE, along with the FWHM in terms of the current density in the inset.

each quantum well along the [0001] growth orientation. Therefore, according to the alignment of the electron quasi-Fermi level and the conduction band, we can predict that the electrons are more evenly distributed across the 5 nm thickness of each quantum well. Meanwhile, we also show the subbands for the wave functions of C1 and HH1 in Figs. 3(a) and 3(b). The computed subbands in Fig. 3(b) demonstrate the two-dimensional density of states is formed even in the thicker quantum well of sample B. Also, we accordingly show the electron concentration profiles in the MQW regions calculated for both samples A and B in Fig. 4, which illustrates that the electrons in the quantum wells for sample B are more uniformly distributed among the quantum wells while more electrons are accumulated at the quantum well/quantum barrier interface for sample A. A more homogenous electron distribution in the quantum wells for sample B is essential to suppressing the Auger recombination rates, as will be shown subsequently.

Fig. 5(a) shows the calculated Auger recombination rates (R_{AR}) and the radiative recombination rates (R_{radi}) in the MQW regions for both samples A and B as a function of the injection current density. Since the volume of the MQW regions for samples A and B is different, it is reasonable to compare the averaged R_{AR} and R_{radi} . The average recombination rates ($R_{average}$) is defined as $R_{average} = \int_0^{t_{QW}} R(x) \times dx / \int_0^{t_{QW}} x \times dx$, where $R(x)$ is the radiative or Auger recombination rates at different locations (x) along the [0001] growth orientation while t_{QW} is the total thickness of the MQW region. Here, the integration step (dx) is set by the mesh site

which has been properly set in our simulations. Fig. 5(a) shows that the R_{AR} increases with the increasing current density for both the samples and the R_{AR} for sample B is always smaller than that for sample A in the whole range of current density. This result indicates the effectiveness of our proposed structure in the suppression of Auger recombination. Moreover, the R_{AR} overtakes R_{radi} for sample A at 145 A/cm², which arises from the strong electron accumulation locally. The even stronger R_{AR} in sample A is the root cause of the lower optical power and larger efficiency droop in Figs. 2(a)–2(d). Nevertheless, the R_{AR} is always smaller than the R_{radi} within the current density range for sample B as demonstrated in Fig. 5(a). Hence, the R_{AR} is suppressed for sample B, which is accountable for the reduced efficiency droop and the improved optical output power when compared to sample A.

It is worth examining the evolutionary details of the relative Auger recombination and radiative recombination of the two samples to deeply understand the operating principles of our proposed structure. The ratios of the Auger recombination rate and the radiative recombination rate of sample B to sample A are presented in Fig. 5(b). It can be seen that in the low current density range below 75 A/cm², the ratio $R_{AR}(B)/R_{AR}(A)$ is smaller than unity but increases with the current density. This can be understood from the fact that the Auger recombination rate of sample B is overall smaller than that of sample A due to the reduced electron density in the proposed structure. However, as the current density increases, the spreading of the electrons and holes in sample A increases more significantly compared to that of sample B.

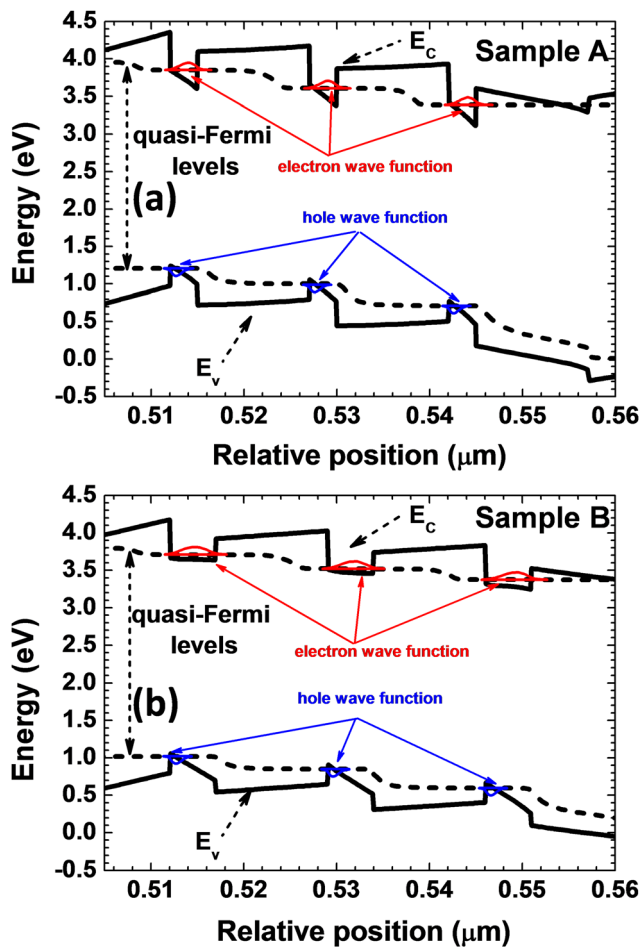


FIG. 3. Computed energy band diagrams for (a) sample A and (b) sample B at 140 A/cm^2 . Here, E_c and E_v mean the conduction band and the valence band, respectively. The subband wave functions (C1 and HH1) are also included.

Therefore, the increasing rate of the Auger recombination in sample A is slower than that in sample B. On the other hand, above the current density of 75 A/cm^2 , due to the thin thickness of sample A, the spreading of the electrons and holes reaches a limit and the carrier density starts to increase quickly, leading to a quick increase of the Auger recombination. This explains the decreasing behavior of the ratio $R_{AR}(B)/R_{AR}(A)$ above 75 A/cm^2 . It should be pointed out

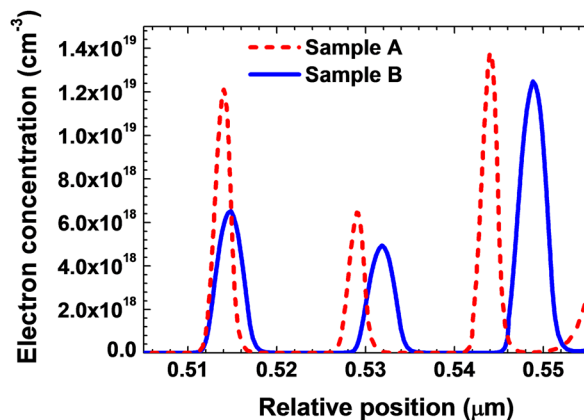


FIG. 4. Computed electron density profiles for (a) sample A and (b) sample B at 140 A/cm^2 .

that the decreasing relative Auger recombination rate does not link to an increase of the relative radiative recombination rate of samples B and A as shown in Fig. 5(b) in the high current density range above 75 A/cm^2 . This could be caused by the more severe current leakage in sample B since the effective conduction band barrier height for electrons has been decreased due to the reduced energy band offset at the $\text{In}_{0.08}\text{Ga}_{0.92}\text{N}/\text{GaN}$ interface. Hence, to suppress both the electron leakage level and Auger recombination simultaneously, it is possible to increase the average InN composition by properly increasing the InN grading level in the quantum wells, as shown in sample B.

In summary, the Auger recombination has been shown to be substantially reduced through linearly varying the InN composition along the [0001] growth orientation in the quantum wells and increasing the quantum well thickness for InGaN/GaN LEDs. The reduction in the Auger recombination is enabled by more evenly distributing the electron profile within the wider quantum wells, which in turn decreases the electron density at high injection current levels. With the proposed quantum well structure embedded into the InGaN/GaN LED, an improved level of optical output power and a reduced efficiency droop have been achieved both numerically and experimentally in this work. Wide InGaN/GaN quantum wells with linearly graded InN

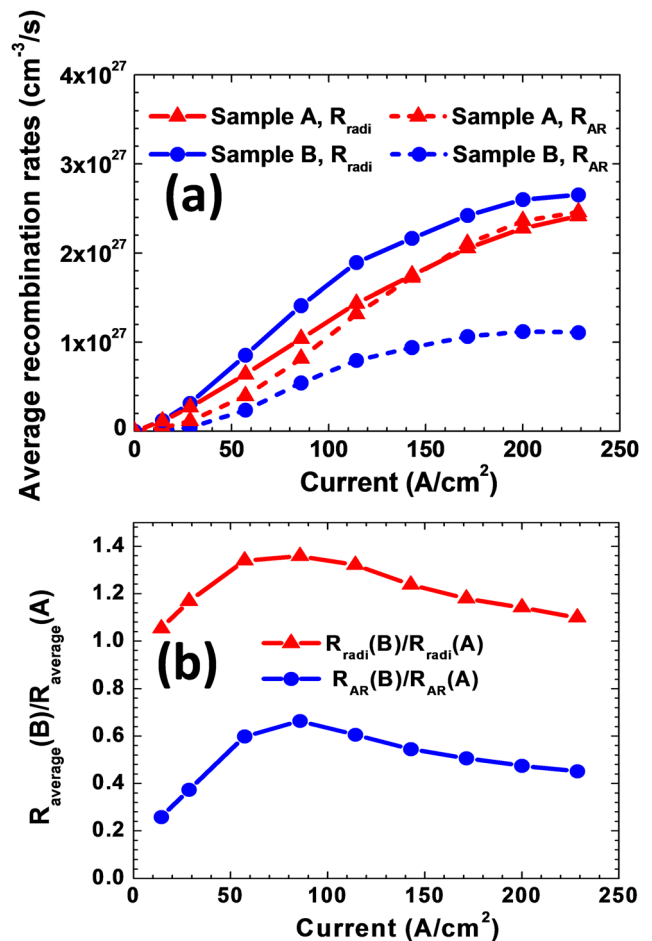


FIG. 5. (a) Averaged Auger and radiative recombination rates for samples A and B and (b) the ratios of the average Auger and radiative recombination rates between samples B and A as a function of the injection current density.

composition hold great promise for achieving high-performance InGaN/GaN LEDs.

This work was supported by the National Research Foundation of Singapore under Grant Nos. NRF-CRP-6-2010-2, NRF-CRP11-2012-01, and NRF-RF-2009-09 and the Singapore Agency for Science, Technology and Research (A*STAR) SERC under Grant No. 112 120 2009.

- ¹S. T. Tan, X. W. Sun, H. V. Demir, and S. P. Denbaars, *IEEE Photonics J.* **4**, 613–619 (2012).
- ²V. Avrutin, S. d. A. Hafiz, F. Zhang, Ü. Özgür, H. Morkoç, and A. Matulionis, *J. Vac. Sci. Technol., A* **31**, 050809 (2013).
- ³Z.-H. Zhang, W. Liu, S. T. Tan, Z. Ju, Y. Ji, Z. Kyaw, X. Zhang, N. Hasanov, B. Zhu, S. Lu, Y. Zhang, X. W. Sun, and H. V. Demir, *Opt. Express* **22**, A779–A789 (2014).
- ⁴G. Verzellesi, D. Saguatti, M. Meneghini, F. Bertazzi, M. Goano, G. Meneghesso, and E. Zanoni, *J. Appl. Phys.* **114**, 071101 (2013).
- ⁵J. Hader, J. V. Moloney, and S. W. Koch, *Appl. Phys. Lett.* **96**, 221106 (2010).
- ⁶E. Kioupakis, P. Rinke, K. T. Delaney, and C. G. Van de Walle, *Appl. Phys. Lett.* **98**, 161107 (2011).
- ⁷Z.-H. Zhang, S. T. Tan, Z. Kyaw, Y. Ji, W. Liu, Z. Ju, N. Hasanov, X. Wei Sun, and H. V. Demir, *Appl. Phys. Lett.* **102**, 193508 (2013).
- ⁸S.-C. Ling, T.-C. Lu, S.-P. Chang, J.-R. Chen, H.-C. Kuo, and S.-C. Wang, *Appl. Phys. Lett.* **96**, 231101 (2010).
- ⁹A. E. Romanov, T. J. Baker, S. Nakamura, J. S. Speck, and E. J. U. Group, *J. Appl. Phys.* **100**, 023522 (2006).
- ¹⁰J.-Y. Chang, F.-M. Chen, Y.-K. Kuo, Y.-H. Shih, J.-K. Sheu, W.-C. Lai, and H. Liu, *Opt. Lett.* **38**, 3158–3161 (2013).
- ¹¹Z.-H. Zhang, S. T. Tan, J. Zhengang, L. Wei, J. Yun, Z. Kyaw, Y. Dikme, X. W. Sun, and H. V. Demir, *J. Disp. Technol.* **9**, 226–233 (2013).
- ¹²Z.-H. Zhang, S. T. Tan, W. Liu, Z. Ju, K. Zheng, Z. Kyaw, Y. Ji, N. Hasanov, X. W. Sun, and H. V. Demir, *Opt. Express* **21**, 4958–4969 (2013).
- ¹³Z.-H. Zhang, S. T. Tan, Y. Ji, W. Liu, Z. Ju, Z. Kyaw, X. W. Sun, and H. V. Demir, *Opt. Express* **21**, 15676–15685 (2013).
- ¹⁴Y. Ji, Z.-H. Zhang, Z. Kyaw, S. T. Tan, Z. G. Ju, X. L. Zhang, W. Liu, X. W. Sun, and H. V. Demir, *Appl. Phys. Lett.* **103**, 053512 (2013).
- ¹⁵Z. G. Ju, W. Liu, Z.-H. Zhang, S. T. Tan, Y. Ji, Z. B. Kyaw, X. L. Zhang, S. P. Lu, Y. P. Zhang, B. B. Zhu, N. Hasanov, X. W. Sun, and H. V. Demir, *Appl. Phys. Lett.* **102**, 243504 (2013).
- ¹⁶V. Fiorentini, F. Bernardini, and O. Ambacher, *Appl. Phys. Lett.* **80**, 1204–1206 (2002).
- ¹⁷Z.-H. Zhang, S. Tiam Tan, Z. Kyaw, W. Liu, Y. Ji, Z. Ju, X. Zhang, X. Wei Sun, and H. V. Demir, *Appl. Phys. Lett.* **103**, 263501 (2013).
- ¹⁸E. Kioupakis, Q. Yan, and C. G. Van de Walle, *Appl. Phys. Lett.* **101**, 231107 (2012).
- ¹⁹J. Piprek and Z. M. S. Li, *Appl. Phys. Lett.* **102**, 131103 (2013).